Available online at www.sciencedirect.com

SCIENCE DIRECT®

Journal of Catalysis 231 (2005) 354–364

JOURNAL OF CATALYSIS

www.elsevier.com/locate/jcat

A kinetic model of CH_4 decomposition and filamentous carbon formation on supported Co catalysts

Yi Zhang, Kevin J. Smith *

Department of Chemical & Biological Engineering, University of British Columbia, 2216 Main Mall Vancouver, BC, Canada, V6T 1Z4

Received 20 October 2004; revised 8 February 2005; accepted 12 February 2005

Available online 23 March 2005

Abstract

A kinetic model of CH_4 decomposition on supported Co catalysts, that describes the stable catalyst activity associated with filamentous carbon formation and the catalyst deactivation associated with the formation of encapsulating carbon, is presented. The rate of carbon nucleation at the tailing face of the supported metal particle, a precursor for the growth of filamentous carbon, is described by a cluster nucleation model. The deactivation or stable activity, observed after an initial rate increase that is associated with carbon nucleation, is explained by the competition between the rate of carbon diffusion through the metal particle and filamentous carbon growth, versus the rate of encapsulating carbon formation on the leading face of the particle. The site density profiles through the metal particle at different reaction times are also calculated, and the effect of metal particle size on the initial CH_4 decomposition rate is quantified.

Keywords: Kinetic model; Methane decomposition; Carbon deposition; Filamentous carbon formation; Carbon nucleation; Encapsulating carbon formation

1. Introduction

Methane decomposition is important in a number of reactions that are intended to convert natural gas to more valuable products with the use of supported metal catalysts. These include CH_4 steam reforming and dry reforming for synthesis gas production and CH_4 homologation for higher hydrocarbon synthesis [1,2]. Catalytic decomposition of CH_4 may also provide an alternative route to H_2 without CO contamination for use with PEM (proton exchange membrane) fuel cells [3], and a cyclic process of CH_4 decomposition at moderate temperature, followed by gasification of carbon with steam or oxygen to produce high-purity H_2 and syngas separately, has also been proposed [4,5]. The production of carbon nanofibres and nanotubes by CH_4 decomposition has also been reported recently [6,7].

The relationship between catalyst deactivation and carbon deposition during decomposition of CH_4 and other hydrocarbons (HCs) is complex and depends on the morphology of the carbon produced. Typically, the carbon forms filaments or nanofibres that act to remove carbon from the active catalyst surface, and this ensures stable activity for extended periods of time. The various rate processes that lead to carbon filament formation and growth during catalytic decomposition of HCs are generally agreed to include (i) deposition of carbon atoms on the exposed surface of the metal catalyst as a consequence of hydrocarbon decomposition, (ii) dissolution and diffusion of carbon through the metal particle, and, finally, (iii) carbon precipitation, nucleation, and filament formation at the back of the metal particle [8–12]. These steps have been included in kinetic models of carbon deposition and filament formation [10–17] over various metal catalysts including Ni, Fe, and Co, and the models have been used to describe the activity-versus-time profiles for metal catalysts. The activity profiles typically show a period of increasing activity that is ascribed to the nucleation of the filamentous carbon followed by a period of steady or declining activity, depending on whether filamentous or encapsulating carbon is produced.

* Corresponding author. Fax: +1 604 822 6003.
E-mail address: kjs@interchange.ubc.ca (K.J. Smith).

0021-9517/$ – see front matter
doi:10.1016/j.jcat.2005.02.010

In catalytic systems, the kinetics of filament formation is dependent on operating conditions, especially temperature and the HC/H_2 ratio in the gas phase, and catalyst properties, including metal particle size [9–17]. On supported catalysts the filament growth occurs between the metal particle and the support, whereas unsupported catalysts allow growth of multiple fibres [18]. Furthermore, as pointed out by De Jong and Geuss [18] and others [11,19], metal–support interaction (MSI) also has an effect on the observed reaction rate. Thus, catalysts prepared by wet impregnation methods on supports that have strong MSI effects will likely behave differently from those prepared by, for example, sputtering [20], where the resulting metal particle will interact less with the support. At very high temperatures (1080 °C) Jourdain et al. [21] have suggested that the metal particle can be split during the formation of carbon nanotubes and have included such a step in their proposed mechanism of carbon nanotube growth.

Carbon nucleation during the formation of filaments corresponds to an observed increase in decomposition activity with time as more filaments nucleate, and this increased activity has been observed in numerous studies [6,7,10,11]. The importance of carbon nucleation during CH_4 decomposition on Ni catalysts has been recognised by Snoeck and coworkers [10,11]. They proposed that the dependence of the number of growing filaments on the affinity of carbon formation must be taken into account in modeling of the kinetics of filamentous carbon formation. Hence, in their study, use of catalysts on which carbon was previously deposited under standard conditions ensured that the rate of growth of the carbon filaments was always based on the same number of filaments. Villacampa et al. [13] have described the kinetics of the nucleation process in a semi-empirical way, assuming the nucleation rate is proportional to the square of a concentration driving force.

Models of the kinetics of carbon nucleation and growth on the surface of substrates relevant to diamond synthesis by CVD processes have been described in the literature [22–24]. In the cluster nucleation model, for example, clusters of carbon atoms are assumed to be more likely to grow than decay once they reach a certain critical size. Nucleation on the surface is the result of collision between mobile single carbon atoms and subcritical clusters, and the nucleation rate corresponds to the rate of addition of single carbon atoms to these subcritical clusters. The rate of growth is determined by the rate of addition of single carbon atoms to the stable clusters. Models of the kinetics of filamentous carbon formation on metal catalysts described in the literature have not included the kinetics of these growth and decay steps associated with nucleation.

In previous work, we reported activity-versus-time profiles for CH_4 decomposition on low loading Co and Ni catalysts at relatively mild temperatures ($\leqslant 500\,^{\circ}C$) [19,25,26]. The catalysts had particle sizes in the range of 8–30 nm. Carbon nanofibres were detected on Co catalysts under conditions similar to those required for nanofibre formation on Ni catalysts [19,25,26]. However, under certain reaction conditions, the stable activity corresponding to carbon nanofibre formation was not obtained, and catalyst deactivation was observed. Furthermore, the activity profiles showed an initial period of increasing activity that was followed by a period of either stable activity or decreasing activity, depending on the reaction conditions, on both supported Ni and Co catalysts [19,25,26]. Since the initial increase in CH_4 decomposition activity is thought to be due to nucleation of carbon filaments, there is a need to include carbon nucleation kinetics in the existing models of CH_4 decomposition kinetics. Furthermore, most models of catalytic carbon filament formation [10,11,14] describe the steady growth of filamentous carbon. For the case of decreasing activity, there are only empirical deactivation models [27,28].

In the present work, a kinetic model of CH_4 decomposition is presented in which the rate of carbon nucleation at the interface between the metal and support is described by the cluster nucleation model. The competition between encapsulating carbon formation and carbon dissolution/diffusion at the surface of the metal is also included to account for catalyst deactivation. The proposed model is fitted to carbon deposition rate data obtained on Co catalysts and partly reported in previous work [25] and to literature data reported for Fe foils [30].

2. Experimental

2.1. Catalysts

The Co/SiO_2 catalysts were prepared by incipient wetness impregnation of a pre-calcined (773 K for 25 h in air) silica support (silica gel, grade 62, 60–200 mesh, 15A, Aldrich 24398-1) according to the procedures described in previous studies [2,25]. The impregnation was followed by drying in vacuum at 373 K for 37 h and then calcining in air at 723 K for 10 min. Before being exposed to reactant, the catalysts were reduced by temperature-programmed reduction (TPR) in 1 h to 923 K in a flow of 40% H_2/Ar at a rate of 100 $ml\,min^{-1}$, and the catalyst metal dispersion was determined by CO chemisorption [26].

2.2. Activity measurements

The CH_4 decomposition activity of the Co catalysts was determined in a fixed-bed microreactor described previously [2,25], with the same experimental procedures and operated in differential mode. Catalyst activity measurements reported here were made under one set of operating conditions. The catalysts were reacted in 23% CH_4/12% H_2/65% Ar at a total gas flow rate of 185 ml (STP)/min at 773 K.

Tests to determine the significance of external and internal diffusional effects were done according to the guidelines given by Froment and Bischoff [29]. For the range of experimental conditions used in the present study, internal and external gradients in concentration and temperature were insignificant [31].

3. Results

3.1. Model development

The kinetic model is applied to the catalyst geometry shown schematically in Fig. 1. The leading face of the catalyst particle refers to the interface between the metal and gas phase, where carbon atoms are formed by the reversible reaction $CH_4 \longleftrightarrow C + 2H_2$. Once the carbon atom is formed, we assume that two parallel and competing processes are possible. The carbon atom can either diffuse through the metal particle and subsequently nucleate and grow filaments at the tailing face (where "tailing face" refers to the interface between the metal and support), or it can form encapsulating carbon on the leading face. We assume that the gasification of encapsulating carbon by H_2 is negligible, and therefore the number of active metal sites at the leading face decreases as encapsulating carbon is produced; this results in catalyst deactivation. This assumption is consistent with the findings of Chen et al. [15] and is supported by results from studies of methane homologation on supported metal catalysts [1,2]. These latter studies have shown that carbon fragments generated from CH_4 are unreactive towards H_2 as they age and as they are exposed to elevated temperatures (> 450 °C). Similarly, it is assumed that the filamentous carbon cannot be gasified in H_2 under the reaction conditions studied. Note, however, that the formation of surface carbon from CH_4 decomposition is reversible, and, consequently, the effects of the CH_4/H_2 ratio and reaction temperature on catalyst deactivation are accounted for indirectly, since this reaction determines the surface carbon concentration, which in turn will govern the rate of encapsulating carbon formation.

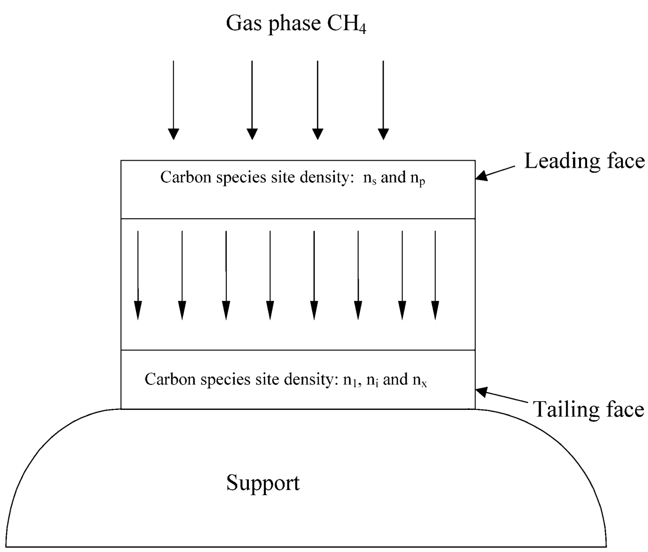

Fig. 1. Schematic of supported metal catalyst geometry used for CH_4 decomposition kinetic model.

The diffusion of carbon through the metal particle is described with a one-dimensional, non-steady-state diffusion equation. Chitrapu et al. [16] have demonstrated that the one-dimensional diffusion equation applied to carbon filament formation gives results similar to those of a two-dimensional model with significantly less computational effort. The driving force for carbon diffusion through the particle is the carbon atom concentration gradient across the particle. A uniform diffusion path length $(2/3)d_p$ was assumed, where d_p is the metal particle diameter, consistent with the average diffusion length in a spherical particle [10, 11,14,15]. Thus, the catalyst geometry is approximated by a metal slab, the sides of which do not participate in the excretion of carbon. This approximation, used in a number of other studies [10,11,15], is appropriate for catalysts prepared by incipient wetness impregnation of porous supports that therefore yield metal particles that interact significantly with the support [6,7,19].

Thus, the model includes five important rate processes: the rates of stepwise CH_4 dehydrogenation and encapsulating carbon formation at the leading face of the particle, the rate of carbon diffusion through the particle, and the rates of carbon nucleation and filament growth at the tailing face of the particle.

3.1.1. Model equations

The model equations are from rate expressions for each of the five rate processes relevant to CH_4 decomposition and filamentous carbon formation. The five rate expressions are linked through carbon balance equations that can be written for both the tailing face and the leading face of the particle. On the leading face of the metal particle, we define the net rate of carbon formation from CH_4 stepwise dehydrogenation and gasification ($CH_4 \longleftrightarrow C + 2H_2$) as $r_f - r_g$ (cm^{-2} s^{-1}), the rate of encapsulating carbon formation as r_e (cm^{-2} s^{-1}), and the rate of carbon bulk diffusion through the metal particle as r_d (cm^{-2} s^{-1}). With n_c defined as the site density of single carbon atoms (cm^{-2}) at any position in the particle, a carbon balance on the leading face of the particle yields

$$\left.\frac{dn_c}{dt}\right|_{x=0} = (r_f - r_g) - r_d - r_e \quad (1)$$

$$\text{at } x = 0 \text{ (the leading face); } t > 0.$$

On the tailing face of the particle, the rate of carbon filament nucleation is defined as r_{nucl} (cm^{-2} s^{-1}) and the rate of filament growth as r_{growth} (cm^{-2} s^{-1}). The change in carbon atom site density at the tailing face must equal the rate of carbon diffusion through the metal at the tailing face r'_d (cm^{-2} s^{-1}) minus the rate of carbon atom consumption by carbon filament nucleation r_{nucl} (cm^{-2} s^{-1}) and growth r_{growth} (cm^{-2} s^{-1}) on the tailing face. Hence,

$$\left.\frac{dn_c}{dt}\right|_{x=2/3d_p} = r'_d - r_{nucl} - r_{growth} \quad (2)$$

$$\text{at } x = (2/3)d_p \text{ (the tailing face); } t > 0.$$

The rate of carbon diffusion through the metal particle (x direction) is described by the unsteady state diffusion equation, written on a carbon atom basis

$$\frac{\partial n_c}{\partial t} = D_s \frac{\partial^2 n_c}{\partial x^2}, \tag{3}$$

with the initial condition

$$n_c\big|_{x=0:2/3d_p} = 0 \quad \text{at } t = 0 \text{ for all } x, \tag{4}$$

where D_s ($cm^2\,s^{-1}$) is the carbon diffusivity through the metal particle. The relevant boundary conditions for Eq. (3) are given by Eqs. (1) and (2). The encapsulating carbon formation step is included in the boundary condition at the leading face to account for catalyst deactivation.

In the present study, the carbon nucleation r_{nucl} ($cm^{-2}\,s^{-1}$) and growth r_{growth} ($cm^{-2}\,s^{-1}$) rates at the tailing face are described by the cluster nucleation model. This model has been successfully applied to the carbon nucleation and growth rates on the surface of substrates relevant to diamond synthesis by CVD processes [22,24]. Eq. (3), together with the initial condition Eq. (4) and the two boundary conditions, Eqs. (1) and (2), represents the mathematical formulation of the kinetic model. Solution of these equations provides a complete description of the rate of CH_4 decomposition and carbon formation as a function of time on stream.

3.1.2. Description of the boundary condition at the leading face

Eq. (1) describes the carbon balance at the leading face of the metal particle that arises from CH_4 stepwise dehydrogenation, carbon gasification, and the formation of encapsulating carbon. Two types of carbon species are assumed to exist at the leading face: atomic carbon with site density n_s (cm^{-2}) and encapsulating carbon with site density n_p (cm^{-2}).

The net rate of carbon deposition $r_f - r_g$ is derived from the known elementary reaction steps for CH_4 stepwise dehydrogenation [1,2,10,11]

$$CH_4 + 2S \longleftrightarrow CH_3S + HS, \tag{5}$$

$$CH_3S + S \longleftrightarrow CH_2S + HS, \tag{6}$$

$$CH_2S + S \longleftrightarrow CHS + HS, \tag{7}$$

$$CHS + S \longleftrightarrow CS + HS, \tag{8}$$

$$2HS \overset{K_H}{\longleftrightarrow} 2S + H_2. \tag{9}$$

Since the activation energy for CH_4 in the gas phase ($CH_4 + 2S \rightarrow CH_3S + HS$, where S represents an active site) is less than that of adsorbed CH_4 ($CH_4S + S \rightarrow CH_3S + HS$) over Group VIII metal catalysts [32], it is reasonable to assume that the first step of CH_4 decomposition can be written as Eq. (5). By assuming that reaction (5) is the slow step, combining reactions (6)–(9) and defining the equilibrium constants K_H and K_{CH_3},

$$K_H = \frac{P_{H_2}[S]^2}{[HS]^2}, \tag{10}$$

$$K_{CH_3} = \frac{[HS]^3[CS]}{[CH_3S][S]^3}, \tag{11}$$

we obtain

$$[HS] = \frac{1}{K_H^{1/2}} P_{H_2}^{1/2}[S], \tag{12}$$

$$[CH_3S] = \frac{1}{K_{CH_3} K_H^{3/2}} P_{H_2}^{3/2}[CS]. \tag{13}$$

Since reaction (5) is the slow step, the net rate of carbon deposition ($r_f - r_g$) is given by

$$r_f - r_g = k_f P_{CH_4}[S]^2 - k_r[CH_3S][HS], \tag{14}$$

which by substitution yields

$$\begin{aligned} r_f - r_g &= k_f P_{CH_4}[S]^2 - k_r \frac{1}{K_{CH_3} K_H^2} P_{H_2}^2[S][CS] \\ &= k_f P_{CH_4}[S]^2 - k_g P_{H_2}^2[S][CS]. \end{aligned} \tag{15}$$

The ensemble size associated with the formation of encapsulating carbon C_P, as described by

$$nC \cdot S \xrightarrow{k_p} nC_P \cdot S \quad \text{with } n = 6, \tag{16}$$

was assumed to be 6 [15]; and the encapsulating carbon formation rate is given by

$$r_e = k_{encap} n_s^n. \tag{17}$$

The ensemble size for encapsulating carbon is not well established, since detailed knowledge of the formation of encapsulating carbon is not available. Values of 3, 6, and 10 have been used in the literature [15,23]. An ensemble size of 6 was shown by Chen et al. [15] to give the best fit to their activity data on Ni catalysts, and in our own studies, $n = 6$ gave a better fit to the reported data than $n = 3$.

The carbon diffusion rate at the leading face is described by

$$r_d = D_s \frac{\partial (n_c/dx)}{\partial x}\bigg|_{x=0} \tag{18}$$

so that the boundary condition at the leading face at $t > 0$ is expressed by

$$\begin{aligned} \frac{dn_C}{dt}\bigg|_{x=0} = \frac{dn_s}{dt}\bigg|_{x=0} &= (r_f - r_g) - r_d - r_e \\ &= k_f P_{CH_4}[S]^2 - k_g P_{H_2}^2[S][CS] \\ &\quad - D_s \frac{\partial (n_C/dx)}{\partial x}\bigg|_{x=0} - k_{encap} n_s^6. \end{aligned} \tag{19}$$

The site conservation was used to calculate [CS]

$$[S] + [CS] + [CH_3S] + [HS] + [C_PS] = [S_0], \tag{20}$$

and assuming that [HS] and $[CH_3S]$ are small

$$[S] + [CS] + [C_PS] = [S_0]. \tag{21}$$

Assuming that the encapsulating carbon occupies the same number of sites as a single carbon atom, the change in the number of active sites is described by

$$\frac{d[S]}{dt} = -(r_f - r_g) + r_d, \tag{22}$$

and the change in sites occupied by encapsulating carbon is described by

$$\frac{d[C_pS]}{dt} = k_{encap} n_s^6. \tag{23}$$

3.1.3. Description of the boundary conditions at the tailing face

The boundary condition at the tailing face describes the carbon balance on the catalyst surface at the interface between the metal and the support. At this interface, the rate of carbon consumption by nucleation and growth of carbon filaments must equal the rate of carbon diffusion through the particle at the tailing face. The carbon nucleation and growth rate at the tailing face were modelled with the cluster nucleation model [22,24]. The Boltzmann nucleation model [23] was also investigated but is not described in detail here, since the cluster nucleation model had fewer parameters and gave a better fit to the data of the present study [31].

According to the cluster nucleation model (CNM), single carbon atoms with site density n_1 diffuse over the surface of the tailing face with surface diffusivity D_1 ($cm^2\,s^{-1}$). The CNM assumes that only single carbon atoms are mobile on the surface. The carbon atoms collide and produce clusters containing j carbon atoms with surface concentration n_j. Furthermore, the clusters are more likely to undergo growth than decay when the cluster size exceeds a critical number i, and n_i is defined as the critical cluster site density at the tailing face. All clusters larger than the critical cluster are considered to be stable, and n_x is the stable cluster site density. To simplify the model, we assume that the rates of nucleation and growth are dominated by single carbon addition processes. Consequently, the nucleation rate corresponds to the addition of single carbon atoms to clusters containing i atoms, and growth corresponds to single carbon atom addition to stable clusters containing x atoms where $x \geqslant i + 1$. The rate of nucleation can then be written as $N_r = \sigma_i D_1 n_1 n_i$ and the rate of growth as $N_g = \sigma_x D_1 n_1 n_x$, where the capture numbers, σ_i and σ_x, are used to describe the diffusion flow of single atoms to critical clusters and stable clusters, respectively [22,24]. The capture numbers are known to vary over a narrow range of values, and here σ_i and σ_x were taken to be 4 and 5, respectively, following Vennables et al. [24]. The size i of the critical cluster was taken as 10, consistent with previous studies [22,23]. Accordingly, the boundary condition at the tailing face is described by the following carbon balance equation:

$$\left.\frac{dn_c}{dt}\right|_{x=(2/3)d_p} = \frac{dn_1}{dt} = r'_d - r_{growth} - r_{nucl} = r'_d - \sigma_x D_1 n_1 n_x - (i+1) N_r. \tag{24}$$

The term, r'_d describes the rate at which single carbon atoms are excreted at the tailing face and is given by

$$r'_d = D_s \left.\frac{\partial(n_c/dx)}{\partial x}\right|_{x=(2/3)d_p}. \tag{25}$$

The term $\sigma_x D_1 n_1 n_x$ describes the cluster growth rate by single carbon addition to stable clusters, and the term $(i+1)N_r$ describes the nucleation rate of single carbon atoms with critical clusters that grow into stable clusters [22,24]. To solve Eq. (24), n_i and n_x must be determined. An expression for n_i in terms of n_1 is available from Zinsmeister's relation [33], written as

$$n_i = \begin{cases} 1/2 n_1 (x_{stable} - i) & x > i, \\ 0 & x < i, \end{cases} \tag{26}$$

where

$$x_{stable} = \sigma_i D_1 \int_0^t n_1 \, dt. \tag{27}$$

Eq. (28) gives the growth rate of critical clusters into stable clusters [22,24], from which n_x can be determined by numerical integration

$$N_r = \frac{dn_x}{dt} = \sigma_i D_1 n_1 n_i. \tag{28}$$

3.1.4. Numerical procedures

The second-order partial differential equation (3), the boundary conditions consisting of the site balance equations at the leading face equation (19), and the tailing face equation (24) constitute the model equations that are solved numerically by the finite-volume method without the assumption of any rate-determining step. Simultaneously, the carbon site density at the tailing face corresponding to each iteration in time was calculated by numerical integration of Eqs. (26)–(28). The bulk diffusivity D_s, surface carbon diffusivity at the tailing face D_1, and reaction rate constants for carbon formation k_f, gasification k_g, and encapsulating carbon formation k_{encap}, were estimated by a fit of the model to the carbon deposition rate data. The Marquardt compromise methodology was used for the parameter estimation.

3.2. Model application

3.2.1. Model fit to CH_4 decomposition rate data on Co/SiO_2 catalysts

The kinetic model was fitted to CH_4 decomposition rates measured on Co/SiO_2 catalysts with different Co loadings under the same CH_4 decomposition conditions, namely $K_M = P_{H_2}^2/P_{CH_4} = 0.033$ atm and $T = 773$ K. The model parameter values estimated from a fit of the model to these data are listed in Table 1. Two typical activity profiles obtained on supported Co catalysts during CH_4 decomposition, which showed steady CH_4 decomposition activity and deactivation, are well described by the model as shown in Figs. 2 and 3, respectively.

Table 1
Effect of metal particle size on model parameters estimated from CH_4 decomposition data measured at 773 K in 23% CH_4/12% H_2/65% Ar at a total gas flow of 185 mL (STP) min^{-1} over Co/SiO_2 catalysts

Parameter	Units	Co wt% of Co/SiO_2 catalyst			
		8	10	12	30
d_p	nm	13.5	17.8	19.4	28.0
$D_s \times 10^{14}$	$cm^2\ s^{-1}$	4.05 ± 0.20	6.08 ± 0.01	5.90 ± 0.23	13.6 ± 0.23
$D_1 \times 10^{16}$	$cm^2\ s^{-1}$	4.54 ± 0.38	6.16 ± 0.02	0.96 ± 0.04	0.52 ± 0.01
$k_f \times 10^{19}$	$Pa^{-1}\ cm^2\ s^{-1}$	14.20 ± 0.42	8.80 ± 0.04	7.02 ± 0.004	4.10 ± 0.16
$k_g \times 10^{22}$	$Pa^{-2}\ s^{-1}\ cm^2$	2.82 ± 0.24	2.11 ± 0.04	0.77 ± 0.0004	0.24 ± 0.001
$k_{encap} \times 10^{75}$	$cm^{10}\ s^{-1}$	17.7 ± 0.64	2.95 ± 0.01	0.55 ± 0.00003	$1.13 \times 10^{-4} \pm 1.01 \times 10^{-7}$
R^2	–	0.68	0.84	0.78	0.92

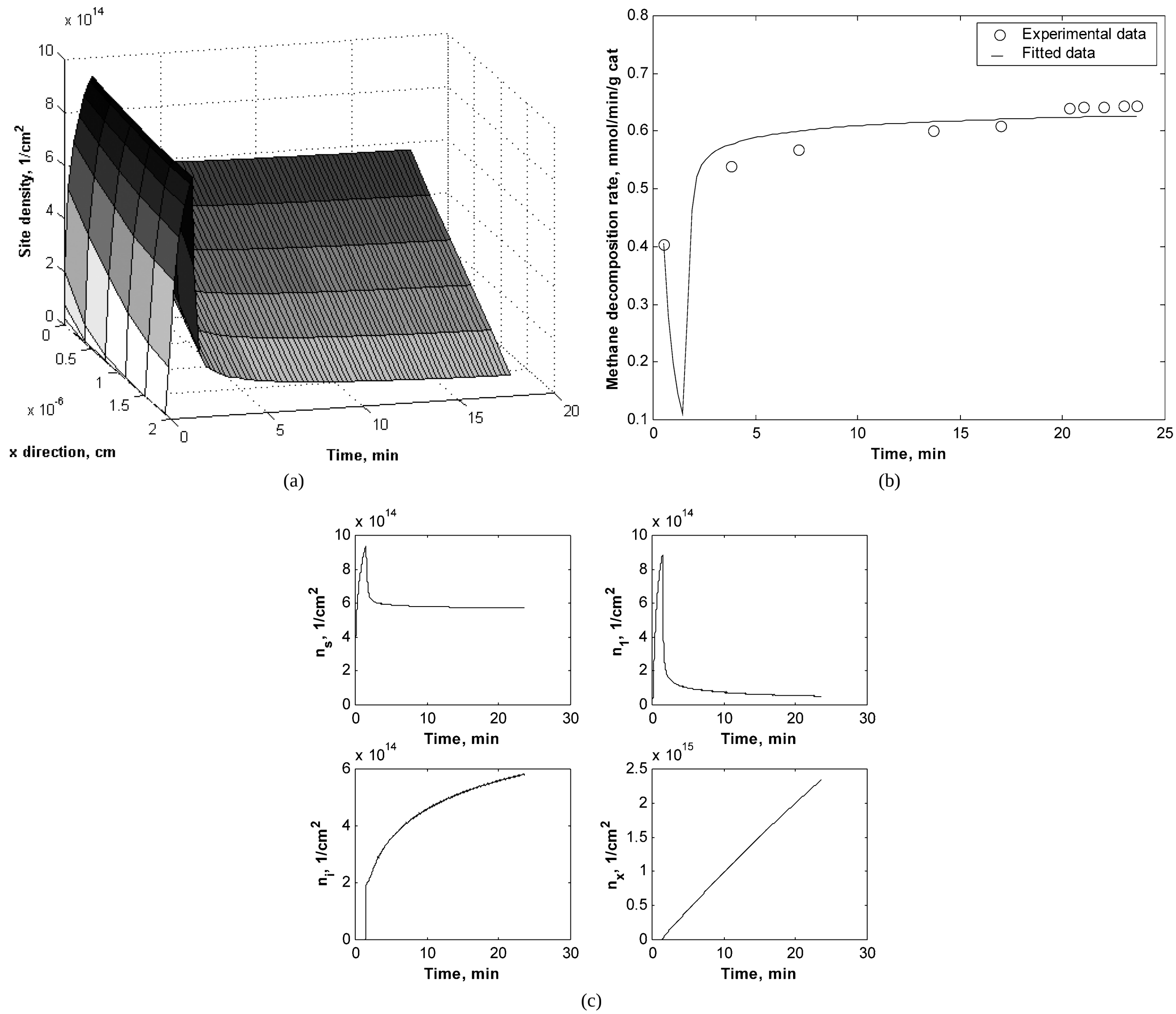

Fig. 2. (a) Calculated carbon site density profile along the diffusion path on 30 wt% Co/SiO_2 catalyst at 773 K in 23% CH_4/12% H_2/65% Ar at a total gas flow of 185 mL (STP) min^{-1} and 101 kPa. (b) Comparison between the carbon deposition rate data measured at 773 K in 23% CH_4/12% H_2/65% Ar at a total gas flow of 185 mL (STP) min^{-1} and 101 kPa on 30 wt% Co/SiO_2 and the carbon deposition rate calculated from the fitted kinetic model. (c) Site density changes as a function of time-on-stream obtained from the kinetic model fit to the carbon deposition rate data measured at 773 K in 23% CH_4/12% H_2/65% Ar at a total gas flow of 185 mL (STP) min^{-1} and 101 kPa on 30 wt% Co/SiO_2.

Figs. 2a–c show the model fit to the CH_4 decomposition rate data on 30 wt% Co/SiO_2 with steady catalyst activity and carbon filament growth. Fig. 2a shows the development of the carbon atom site density profile through the Co metal particle with time on stream. Before the start of carbon nucleation at the tailing face of the particle, the site density increases through the particle as the diffusion driving force decreases because of the accumulation of single carbon atoms at the tailing face of the metal particle. The site density begins to decrease once carbon nucleation and growth at the tailing face begin, however, and this decrease means that the driving force for carbon diffusion through the particle increases again. Finally, the profile stabilises, corresponding to stable filament growth at the tailing face. The carbon deposition rate with respect to time on stream on the metal Co particle calculated by the model is compared with the measured data in Fig. 2b. The model calculates an initial rate decrease, followed by an increase in rate and finally stable activity. The period corresponding to the initial rate decrease is associated with non-steady-state carbon diffusion through the metal and the accumulation of single carbon atoms at the tailing face of the particle before the start of nucleation. The subsequent period of rate increase corresponds to carbon nucleation. The final, stable carbon deposition rate corresponds to the steady growth of carbon filaments. Note that although the steady growth of carbon nanofibres after the rate increase associated with nucleation was well described by the model, as shown in Fig. 2b, the rapid decline in activity before the start of nucleation was not observed. The CH_4 decomposition rate data were measured at intervals of 3.3 min [31], whereas the model suggests that under the reaction conditions of Fig. 2b, the nucleation process was completed within this time interval. Data in Fig. 2c show the changes in n_s, n_1, n_i and n_x with time on stream. The three stages identified in Fig. 2 correspond to the following rate processes. Stage (i) corresponds to non-steady-state diffusion, n_1 increases, and n_i and n_x are equal to zero since single carbon atoms are only accumulating at the tailing face but have not yet begun to nucleate. Consequently, the carbon diffusion rate at the tailing face is low. In stage (ii), carbon nucleation and growth have begun, so that n_1 decreases, whereas n_i and n_x increase. Consequently, the carbon diffusion rate increases because the driving force for carbon diffusion increases. Finally in stage (iii), the rate of carbon nucleation and growth at the tailing face and carbon diffusion rate through the particle reach steady values.

Figs. 3a–c show the fit of the model to the CH_4 decomposition rate on 10 wt% Co/SiO_2, with catalyst deactivation after the initial rate increase. The site density profiles along the metal particle at different reaction times (Fig. 3a) again show the presence of various stages of reaction during CH_4 decomposition. Fig. 3b shows that the catalyst deactivation was also well described by the kinetic model. Under the reaction conditions of Fig. 3b, however, the initial diffusion of carbon through the catalyst occurs rapidly, and only the subsequent nucleation stage is apparent from the data. Furthermore, catalyst deactivation occurs because of a high rate of formation of encapsulating carbon (Table 1).

4. Discussion

4.1. Model fit to selected literature data

As mentioned above, the nucleation rate, the rate of steady growth of carbon nanofibres, and the rate of deactivation after nucleation were all well described by the model. However, as shown in Fig. 3b, the brief period at the start of the reaction, in which the model predicts a rapid decline in activity corresponding to non-steady-state diffusion before the start of nucleation, was not observed experimentally on the Co catalysts. The experimental procedure used to measure CH_4 decomposition rates in the present study relied on sampling the reactor exit gas at a period of about 3.3 min [31]. The brief period before nucleation lasted less than 3 min under the conditions of Fig. 2 and, consequently, was not observed. However, initial carbon deposition rate data can be calculated from the experimental results reported by Sacco et al. [30] for Fe foil at 900 K. The kinetic model can then be fitted to these data, once the active surface area and hence the initial surface site density are known. Note that although other CH_4 decomposition data are available in the literature, including recent data on Co catalysts, these data do not give the carbon deposition in the first few minutes of reaction [6,7] or they do not report the catalyst active surface area [14,15].

Fig. 4 shows two sets of carbon deposition rate data that were calculated from data reported by Sacco et al. [30] on $6 \times 6 \times 0.25$ mm polycrystalline Fe foil at 900 K during the first 30 min of reaction. The data of Sacco et al. provided weight change measurements of the Fe foil at 30-s intervals from the beginning of the deposition process. The values of Fig. 5 were obtained by differentiation of the cumulative weight gain data reported in [30]. Note that Fig. 5 shows evidence of an initial stage of activity decline for one of the two sets of data. For both sets, the activity profile shows a period when the rate increases, presumably because of the nucleation process. These results also suggest that the initial period of rate decline is only observed when the nucleation process is slow relative to the diffusion rate. The short, initial period during which the rate of carbon deposition decreases has also been observed in more recent studies over Fe catalysts [7,12], and in both cases this phenomenon is observed only under particular operating conditions.

The kinetic model of the present study was fitted to the rate data of Fig. 5, corresponding to the partial pressures $P_{CO}P_{H_2} = 0.13\ \text{bar}^2$, $P_{CO_2}/P_{CO}^2 = 0.21\ \text{bar}^3$, and for which the three stages of filament formation were apparent. However, because the reactant gas included CO and CO_2 and the kinetics of the surface reaction involving these species is complex, it was assumed that n_s was fixed at the leading face during the reaction. Furthermore, encapsulating carbon

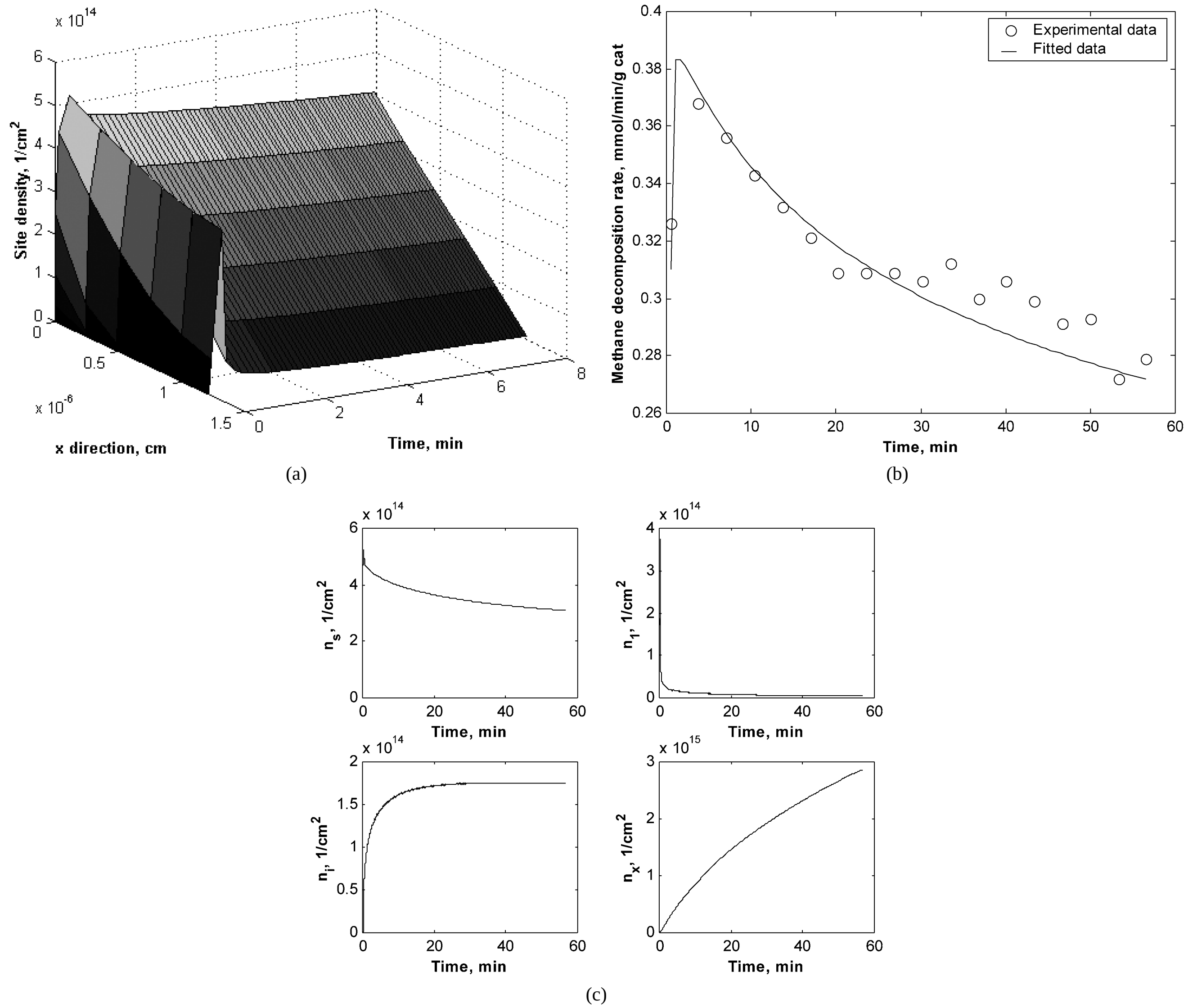

Fig. 3. (a) Calculated carbon atom profile along the diffusion path with steady carbon growth on 10 wt% Co/SiO_2 catalyst at 773 K in 23% CH_4/12% H_2/65% Ar at a total gas flow of 185 mL (STP) min^{-1} and 101 kPa. (b) Comparison between the carbon deposition rate data measured at 773 K in 23% CH_4/12% H_2/65% Ar at a total gas flow of 185 mL (STP) min^{-1} and 101 kPa on 10 wt% Co/SiO_2 and the carbon deposition rate calculated from the fitted kinetic model. (c) Site density changes as a function of time-on-stream obtained from the kinetic model fit to the carbon deposition rate data measured at 773 K in 23% CH_4/12% H_2/65% Ar at a total gas flow of 185 mL (STP) min^{-1} and 101 kPa on 10 wt% Co/SiO_2.

formation at the leading face was neglected because stable activity was obtained after carbon nucleation. Accordingly, by fitting the carbon deposition rate data to the model, we estimated the bulk carbon diffusivity D_s, the surface carbon diffusivity at the tailing face D_1, and the site density of single carbon atoms at the leading face n_s. The fitted parameters are listed in Table 2; with these parameter values, the site density profiles and the CH_4 decomposition rates were calculated as shown in Figs. 5a–c.

The three stages shown in Fig. 5 can be well explained by the proposed kinetic model. The initial rate decrease corresponds to the initial, non-steady-state carbon diffusion during which carbon clusters of critical size i have not yet formed on the tailing face of the catalyst particle. During this period, the carbon diffusion rate decreases with time on stream because single carbon atoms accumulating at the tailing face have not yet been excreted from the particle, and, consequently, the driving force for carbon diffusion (the difference in the concentration of single carbon atoms between the leading face and the tailing face of the particle) decreases with time on stream. As carbon diffusion proceeds, the single carbon atoms at the tailing face start to nucleate and grow. During this period, the site density of single carbon atoms at the tailing face decreases and the driving force for carbon diffusion increases. Hence, the observed carbon deposition rate increases for a period corresponding to carbon nucleation. Eventually, stable activity corresponding to steady carbon growth is observed. The carbon site density profiles in Fig. 5a also show three distinct stages corresponding to non-steady-state diffusion, carbon nucleation,

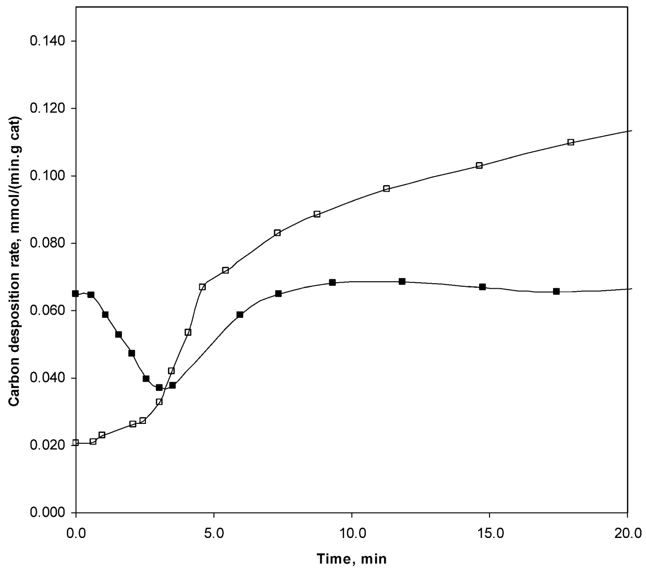

Fig. 4. Carbon deposition rate versus time for various H_2, CO, CO_2, CH_4 and H_2O partial pressures at 900 K and 1 bar over Fe foil. Data calculated from [30]. (■, $P_{CO}P_{H_2} = 0.13$ bar^2, $P_{CO_2}/P_{CO}^2 = 0.21$ bar^3; □, $P_{CO}P_{H_2} = 0.12$ bar^2, $P_{CO_2}/P_{CO}^2 = 2.0$ bar^3).

and, finally, steady growth of carbon nanofibers, as described previously. Fig. 5b shows that the steady growth of carbon nanofibres after the initial rate increase was well described by the model.

The modeling results of Table 2 provide estimates of D_s. Over Fe foil at 900 K, $D_s = 2.7 \times 10^{-6}$ cm^2 s^{-1} was obtained. Values of carbon diffusivity in Fe reported in the literature vary over several orders of magnitude. Safvi et al. [34] demonstrated that carbon diffusivity is dependent upon the carbon activity, reporting that diffusivity increased from 1×10^{-9} to 1×10^{-6} cm^2 s^{-1} as carbon activity increased from 0 to 35 on γ-Fe at 1033 K. Extrapolation of data summarised by Yokoyama et al. [35] yields values of 5×10^{-9} cm^2 s^{-1} at 900 K for γ-Fe, but the carbon activity was not reported in this case. The value of D_s over Fe foil at 900 K estimated from the kinetic model is high but within the range of literature values.

4.2. Effect of metal particle size

Table 1 summarises the estimated model parameter values obtained for the series of Co/SiO_2 catalysts, each with a different particle size. Values of D_s, the carbon diffusivity in the Co, in the range of 4.05×10^{-14} to 1.36×10^{-13} cm^2 s^{-1} were obtained. Few data are available for carbon diffusivity in Co at the temperature of the present study. Extrapolation of the data summarised by Yokoyama et al. [35] yields $D_s = 6.94 \times 10^{-12}$ cm^2 s^{-1} for carbon diffusion through a Co foil, one to two orders of magnitude larger than the values obtained from the kinetic model (Table 1). Safvi et al. [34] demonstrated that carbon diffusivity is dependent upon the carbon activity and reported that diffusivity increased from 1×10^{-9} to 1×10^{-6} cm^2 s^{-1} as carbon activity increased

Table 2
Estimated model parameters for the kinetic model applied to carbon decomposition data reported by Sacco et al. [30] and measured on Fe foil at 900 K and $P_{CO}P_{H_2} = 0.13$ bar^2, $P_{CO_2}/P_{CO}^2 = 0.21$ bar^3

$n_s \times 10^{-17}$ (cm^{-2})	$D_s \times 10^6$ (cm^2 s^{-1})	$D_1 \times 10^{20}$ (cm^2 s^{-1})	F-Statistic
6.64 ± 0.04	2.66 ± 0.02	7.70 ± 0.02	14.6

from 0 to 35 on γ-Fe at 1033 K. The difference between the values obtained in the present study and those extrapolated from the study of Yokohama et al. is possibly also due to activity differences. In the present study, the carbon activity of the gas phase was approximately 7.0, whereas the carbon activity was not reported by Yokoyama et al. [35].

The modeling results of Table 1 also showed that D_s increased with increasing metal particle size. One possible explanation for this observation is the influence of the exposed surface plane on carbon diffusion rate. Both (100) and (110) surfaces are more suited for carbon diffusion [36] and are apparently favoured at the gas/metal interface, whereas the (111) face is favoured at the graphite/metal interface of α-Fe, Co, and Ni catalysts [35]. In the present study, the decrease in carbon diffusivity, D_s, with decreasing metal particle size may also be influenced by the fact that (100) and (110) faces are less favourable for small metal particles.

Modeling results of Table 1 also showed that the carbon surface diffusivity, D_1, decreased with increasing metal particle size, resulting in a weaker ability for carbon nucleation. Finally, the rate constant of encapsulating carbon formation, k_{encap}, decreased with increasing metal particle size. Yang and Chen [36] reported that encapsulating carbon formation on Ni was also dependent on the exposed surface, with encapsulating carbon favouring binding on Ni (111), followed in order by (111) > (311) > (100) > (110). In the present study the decrease in k_{encap} with increasing metal particle size may also be a result of the low-index planes (100) and (110) being dominant on the large crystallites of the supported Co catalysts.

In the present study, the initial forward rate of methane decomposition (initial TOF, s^{-1}) was obtained from the value of k_f and the exposed metal surface area as estimated from CO uptake measurements [25] with the equation $r_f = k_f P_{CH_4}[S]^2$. The calculated values, plotted versus metal particle size in Fig. 6, show that the initial forward rate of CH_4 decomposition decreased as metal particle size increased. This result is in agreement with results of Wei and Iglesia [37,38], who demonstrated that the forward CH_4 turnover frequency (TOF) for CH_4–H_2O, CH_4–CO_2, and CH_4 decomposition reactions decrease with increasing metal particle size. Wei and Iglesia [37,38] suggested that the coordinatively unsaturated surface atoms prevalent in small crystallites are significantly more active than those in the low-index planes predominately exposed on large crystallites, and similar effects have been predicted theoretically for model metal surfaces by Szuromi et al. [39]. Note that

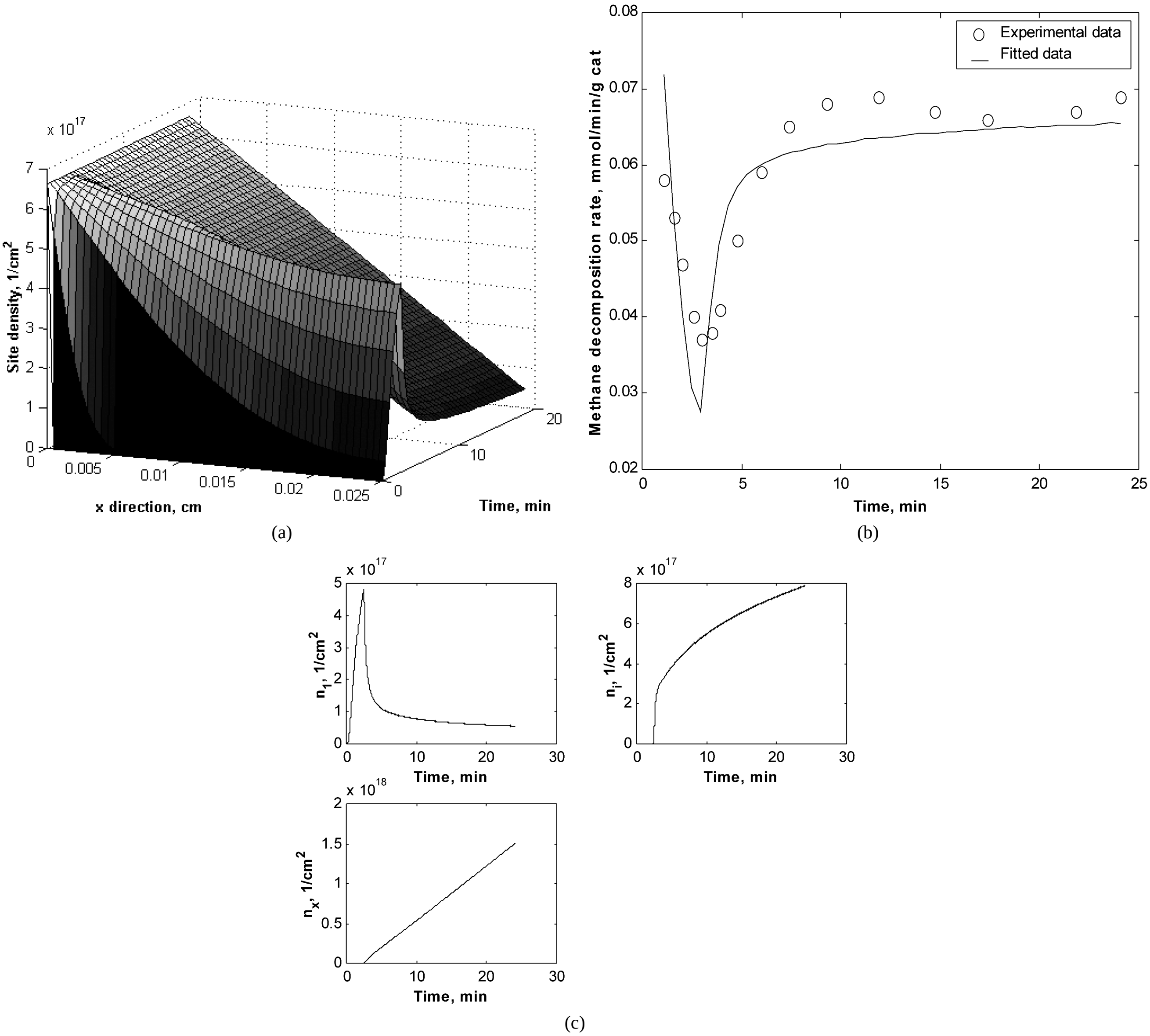

Fig. 5. (a) Single carbon atom profile along the depth of Fe foil obtained by fitting carbon deposition rate data at $P_{CO}P_{H_2} = 0.13\ \text{bar}^2$, $P_{CO_2}/P_{CO}^2 = 0.21\ \text{bar}^3$, 900 K and 1 bar [30] to the cluster nucleation model. (b) Comparison between the measured carbon deposition rate data obtained at $P_{CO}P_{H_2} = 0.13\ \text{bar}^2$, $P_{CO_2}/P_{CO}^2 = 0.21\ \text{bar}^3$, 900 K and 1 bar on Fe foil [30] and the carbon deposition rate calculated from the fitted kinetic model. (c) Site density changes as a function of time-on-stream obtained from the model fit to the literature carbon deposition rate data [30] measured at $P_{CO}P_{H_2} = 0.13\ \text{bar}^2$, $P_{CO_2}/P_{CO}^2 = 0.21\ \text{bar}^3$, 900 K and 1 bar.

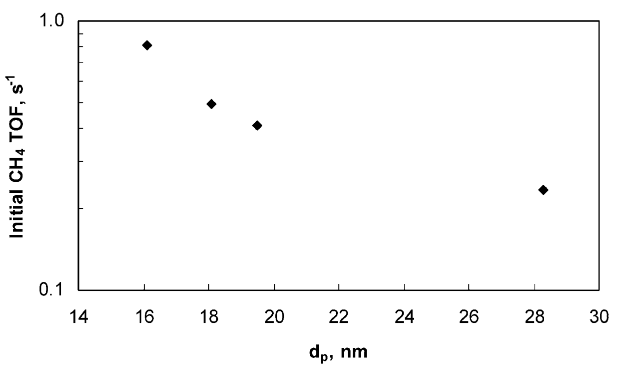

Fig. 6. Effect of metal particle size on the initial forward TOF for CH_4 decomposition on Co/SiO_2 catalysts at 773 K and 101 kPa.

the initial forward rates of methane decomposition (initial TOF, s^{-1}) obtained from the kinetic model are different from the maximum methane decomposition activity, r_0, reported previously [25] and determined by correlation of the activity versus time profile with the equation $r = r_0 e^{k_d t}$, where r is the measured CH_4 decomposition activity, r_0 is the maximum activity, and k_d is the deactivation constant. As the kinetic model shows, the maximum methane decomposition rate is that measured after nucleation. Consequently, r_0 was shown to decrease as the Co and Ni dispersion increased or the metal particle size decreased [19,25], because the rate increases as the number of nuclei increases with metal particle size.

5. Conclusions

A kinetic model of CH_4 decomposition on supported Co catalysts has been presented that describes the stable activity associated with carbon nanofibre formation and catalyst deactivation associated with the formation of encapsulating carbon. The initial increase in activity was described by a cluster nucleation model at the tailing face of the metal particle. The model was shown to fit carbon deposition rate data and identified three stages of carbon deposition. Initially, activity declined as the carbon concentration increased at the tailing face of the metal particle, leading to a reduced carbon diffusion rate through the metal particle. The rate then increased as carbon nucleation occurred. Subsequently, either stable activity was observed as carbon filaments continued to grow, or deactivation was observed as encapsulating carbon was produced on the leading face of the metal particle. The Co particle size was shown to play an important role in the CH_4 decomposition activity, with smaller metal particles favouring increased initial CH_4 decomposition TOFs, and larger metal particles favouring stable CH_4 decomposition and filament formation.

Acknowledgments

Funding for the present study from the Natural Sciences and Engineering Research Council of Canada is gratefully acknowledged.

References

[1] T. Koerts, M.J.A.G. Deelen, R.A. van Santen, J. Catal. 138 (1) (1992) 101.
[2] J.S.M. Zadeh, K.J. Smith, J. Catal. 176 (1) (1998) 115.
[3] T.V. Choudhary, D.W. Goodman, Catal. Today 77 (1–2) (2002) 65.
[4] T.J. Zhang, M.D. Amiridis, Appl. Catal. A: Gen. 167 (2) (1998) 161.
[5] V.R. Choudhary, S. Banerjee, A.M. Rajput, J. Catal. 198 (1) (2001) 136.
[6] S. Takenake, M. Ishida, M. Serizawa, E. Tanabe, K. Otsuka, J. Phys. Chem. B 108 (2004) 11464.
[7] S. Takenaka, M. Seizawa, K. Otsuka, J. Catal. 222 (2004) 520–531.
[8] C.H. Bartholomew, Appl. Catal. A: Gen. 212 (1–2) (2001) 17.
[9] J. Rostrup-Nielsen, D.T. Trimm, J. Catal. 48 (1977) 1155.
[10] J.W. Snoeck, G.F. Froment, M. Fowles, J. Catal. 169 (1) (1997) 240.
[11] J.W. Snoeck, G.F. Froment, M. Fowles, J. Catal. 169 (1) (1997) 250.
[12] W. Arabczyk, W. Konicki, U. Narkiewicz, I. Jasinsak, K. Kalucki, Appl. Catal. 266 (2004) 135.
[13] J.I. Villacampa, C. Royo, E. Romeo, J.A. Montoya, P. Del Angel, A. Monzon, Appl. Catal. A: Gen. 252 (2003) 363.
[14] M. Perez-Cabero, E. Romeo, C. Royo, A. Monzon, A. Guerrero-Ruiz, A. Rodriguez-Ramo, I. Rodriguez-Ramo, J. Catal. 224 (2004) 197–205.
[15] D. Chen, R. Lodeng, A. Anundskas, O. Olsvik, A. Holmen, Chem. Eng. Sci. 56 (4) (2001) 1371.
[16] P. Chitrapu, C.R.F. Lund, J.A. Tsamopoulos, Carbon 30 (2) (1992) 285.
[17] I. Alstrup, M.T. Tavares, J. Catal. 139 (1993) 513.
[18] K.P. De Jong, J.W. Geus, Catal. Rev. 42 (4) (2000) 481.
[19] X. Li, Y. Zhang, K.J. Smith, Appl. Catal. A: Gen. 264 (2004) 81.
[20] C. Ducati, I. Alexandra, M. Chhowalla, J. Robertson, G.A.J. Amaratunga, J. Appl. Phys. 95 (2004) 6387.
[21] V. Jourdain, H. Kanzow, M. Castignolles, A. Loiseau, P. Bernier, Chem. Phys. Lett. 364 (2002) 27.
[22] H.M. Liu, D.S. Dandy, J. Electrochem. Soc. 143 (3) (1996) 1104.
[23] M. Grujicic, G. Cao, B. Gersten, Mat. Sci. Eng. B SOLID 94 (2–3) (2002) 247.
[24] J.A. Venables, G.D.T. Spiller, N. Hanbucken, Rep. Prog. Phys. 47 (1984) 399.
[25] Y. Zhang, K.J. Smith, Catal. Today 77 (2002) 257.
[26] Y. Zhang, K.J. Smith, Catal. Lett. 95 (1–2) (2004) 7.
[27] M.C. Demicheli, E.N. Ponzi, O.A. Ferretti, A.A. Yeramian, Chem. Eng. J. Biochem. Eng. 46 (3) (1991) 129.
[28] G.G. Kuvshinov, Y.I. Mogilnykh, D.G. Kuvshinov, Catal. Today 42 (3) (1998) 357.
[29] G.F. Froment, K.B. Bischoff, Chemical Reactor Analysis and Design, second ed., Wiley, New York, 1990.
[30] A. Sacco, P. Thacker, T.N. Chang, A.T.S. Chiang, J. Catal. 85 (1984) 224.
[31] Y. Zhang, PhD thesis, The University of British Columbia (2004).
[32] E. Shustorovich, A.T. Bell, Surf. Sci. 248 (3) (1991) 359.
[33] G. Zinsmeister, Thin Solid Films 4 (1969) 363.
[34] S.A. Safvi, E.C. Bianchini, C.R.F. Lund, Carbon 29 (8) (1991) 1245.
[35] H. Yokoyama, H. Numakura, M. Koiwa, Acta Mater. 46 (8) (1998) 2823.
[36] R.T. Yang, J.P. Chen, J. Catal. 115 (1989) 52.
[37] J. Wei, E. Iglesia, J. Catal. 224 (2004) 370.
[38] J. Wei, E. Iglesia, J. Catal. 225 (2004) 116.
[39] P.D. Szuromi, J.R. Engstrom, W.H. Weinberg, J. Phys. Chem. 89 (1985) 2497.